Proceedings IRF2018: 6th International Conference Integrity-Reliability-Failure
Lisbon/Portugal 22-26 July 2018. Editors J.F. Silva Gomes and S.A. Meguid
Publ. INEGI/FEUP (2018); ISBN: 978-989-20-8313-1

PAPER REF: 7074

FRACTURE MECHANICS ANALYSIS OF POROSITY EFFECT ON STRENGTH CHARACTERISTICS OF POROUS ALUMINA

Natsumi Miyazaki(*), Toshihiko Hoshide

Department of Energy Conversion Science, Kyoto University, Kyoto, Japan
(*)*Email:* miyazaki.natsumi.35z@st.kyoto-u.ac.jp

ABSTRACT

In this work, bending strength properties of porous alumina were investigated to clarify porosity effects on strength. Three-point bending tests were conducted by using alumina with three different porosities as well as dense one. It was revealed that the bending strength decreased drastically as increasing porosity. Cross sections were observed through a laser scanning microscope to characterize spatial and size distributions of pores. In this study, based on the observed pore characteristics, a fracture mechanics procedure was proposed by presuming pores to be surrounded by virtual cracks with specific length. Monte Carlo simulations based on the proposed procedure were carried out by assuming the same properties of virtual-crack distribution as those of pore distribution observed in a material. Strength simulated by using the proposed procedure almost coincided with experimentally observed one. Consequently, the proposed procedure was confirmed to be efficient in evaluating effects of porosity and pore-distributions on strength of porous alumina.

Keywords: porous alumina, fracture mechanics, porosity, statistical strength-properties, pore distribution.

INTRODUCTION

Porous ceramics have higher heat-resistance and larger specific surface area. Therefore, porous ceramics are expected to be applied to filters and catalysts in energy related components. Strength properties of porous ceramics should be appropriately evaluated to guarantee long-term durability, even if their applications are functional ones. In previous works on porous ceramics, compressive strength but not tensile one was investigated at first (Eugene, 1953), and then subsequent works were focused on bending strength (Hoshide, 1988; Kawai, 1997). A relation between bending strength and porosity was examined (Hoshide, 1988), but the range of investigated porosity was limited around 10% or less. Strength tests using porous ceramics with systematically changed porosity are required so that correlation of strength with respect to porosity variation can be discussed fundamentally.

In general, strength is expected to become lower in a ceramic material with higher porosity. It should be taken into account, however, that not only bulk porosity but also spatial and size distributions of pores must affect strength properties of porous ceramics. There is no previous study that strength properties of porous ceramics are investigated by considering such pore-distributions.

In this work, alumina ceramics having various porosities were selected as one of porous ceramic materials, and strength properties of porous alumina were investigated by experiments and simulations. The influence of spatial and size distributions of pores on

strength properties was experimentally clarified by conducting bending tests using smooth specimens of porous alumina. Cross sections were observed through a laser scanning microscope (LSM) to characterize spatial and size distributions of pores. A fracture mechanics procedure was proposed by considering the observed pore characteristics and by presuming pores to be surrounded by virtual cracks. Simulations on strength of numerous samples were also executed based on the proposed procedure, and statistical distributions of strength were discussed by applying Weibull distribution functions.

EXPERIMENTAL PROCEDURES

Materials and specimen preparations

Materials used in this work were commercial porous alumina ceramics with three different porosities p = 34.9%, 48.4% and 57.8%. A dense alumina with 0.803% porosity was also prepared as a reference material. The materials are respectively named as AL-01, AL-35, AL-48 and AL-58, according to percentage values of porosity. Physical properties of the materials are summarized in Table 1.

Table 1 - Physical properties of alumina ceramics

Material	**AL-01**	**AL-35**	**AL-48**	**AL-58**
Porosity *p* (%)	0.803	34.9	48.4	57.8
Bulk density (Mg/m^3)	3.95	2.59	2.05	1.68
Water absorption (%)	0.00	13.9	30.0	35.0
Purity (%)	99.7	99.5~	97.0~	88.0

Specimens were machined into square-bar having a width of 4mm, a thickness of 3mm, and a length of 40mm, which are the same as the standard bending specimen specified in JIS R 1601 (2008).

Bending test

All bending tests were conducted under three-point bending mode with a span length of 20mm in an ambient atmosphere, i.e. 294±5K and 40±14% relative humidity. The loading rate was controlled so that the rate of the maximum tensile stress in a specimen might be about 100MPa/s. The bending strength of a specimen was evaluated as the maximum stress monitored at its fracture.

Evaluation of apparent fracture toughness

An apparent fracture toughness was obtained by applying straight-notched specimens to 3-point bending test. A straight-notch has a width of 2.4mm and a depth of 2mm for porous materials, and a width of 0.55mm and a depth of 23μm for dense material, respectively. The condition in bending test was the same as one as mentioned above.

EXPERIMENTAL RESULTS AND DISCUSSION

Bending strength

Figure 1 presents relation between porosity p and bending strength σ_f. As seen in Figure 1, bending strength is decreased drastically with increase in p. The relation is adequately approximated by the next exponential function of p.

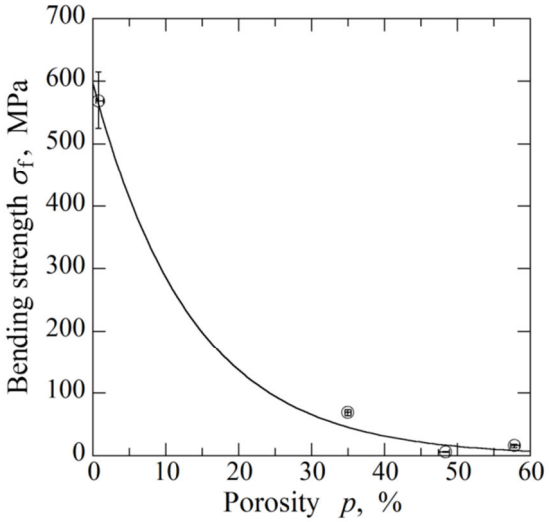

Fig. 1 - Relation between bending strength and porosity

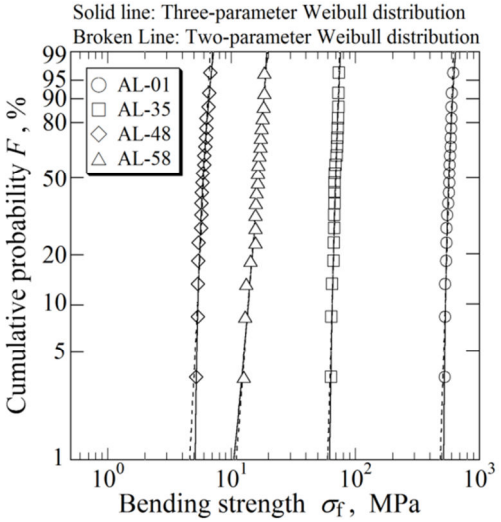

Fig. 2 - Weibull plot of bending strength

$$\sigma_f = 598 \exp(-0.0735\, p) \tag{1}$$

It is well known that large scatters are observed in strength properties of brittle materials such as ceramics. A statistical distribution of strength in ceramic material is approximated by using Weibull distribution function (Weibull, 1939). Weibull distribution function for random variable x is defined as a cumulative probability function $F(x)$ as follows.

$$F(x) = 1 - \exp\left[-\left(\frac{x - x_L}{x_S} \right)^{\alpha} \right] \tag{2}$$

In the above equation, parameters x_L, x_S and α are respectively location parameter, scale parameter and shape parameter. Two-parameter Weibull distribution function is given by setting $x_L = 0$ in (3). In statistical analyses, σ_f is treated as a random variable x in (2). Figure 2 presents distributions of strength σ_f in respective materials, which are plotted in a Weibull probability paper. The solid curved lines in Figure 2 represent the cumulative probability functions $F(x)$, which are fitted to three-parameter Weibull distribution function. The broken straight lines in Figure 2 show relations fitted to two-parameter functions. Although porosity of AL-58 is higher than that of AL-48, Figure 2 represents that the strength distribution of AL-58 is in higher strength region compared with that of AL-48. Such a suspicious trend is suggested to be caused by difference in spatial and size distributions of pores. This will be further discussed by simulation taking account of such distributions in the next chapter.

The statistics of bending strength σ_f are summarized in Table 2. The table also includes scale parameter $\sigma_{f,S}$, scale parameter α and location parameter $\sigma_{f,L}$, which were obtained by fitting strength distribution to Weibull distribution function. Table 2 shows that, as increasing porosity, the coefficient of variation becomes larger and the shape parameter in two-parameter Weibull distribution function is smaller. This implies that a relative scatter of strength is increased in a material with higher porosity.

Table 2 - Statistical parameters of bending strength

Material		AL-01	Al-35	AL-48	AL-58
Average strength $\sigma_{f,ave}$ (MPa)		569	69.0	5.91	16.1
Coefficient of variation COV		0.0462	0.0426	0.0732	0.106
Parameters in two-parameter Weibull distribution	Scale parameter $\sigma_{f,S}$ (MPa)	580	70.4	6.10	16.9
	Shape parameter α	25.4	27.5	16.0	10.5
Parameters in three-parameter Weibull distribution	Scale parameter $\sigma_{f,S}$ (MPa)	72.5	12.7	1.07	39.8
	Shape parameter α	2.36	4.23	2.20	26.3
	Location parameter $\sigma_{f,L}$ (MPa)	505	57.5	4.95	–23.0

Apparent fracture toughness

Table 3 shows apparent fracture toughness $K_{C,ap}$ for respective materials, which were measured by using the procedure mentioned above. These values almost qualitatively satisfy the tendency in the relation of fracture toughness versus bending strength in the alumina (Hoshide, 1998). It should be remarked, however, that these overestimates actual fracture toughness because the straight notch used in bending specimen is not a crack. Fracture toughness K_{Cp}, which will be theoretically estimated in the next chapter, is also listed in Table 3.

Table 3 - Fracture toughness values in respective materials

Material	AL-01	AL-35	AL-48	AL-58
Measured apparent fracture toughness $K_{C,ap}$ (MPa·m$^{1/2}$)	4.05	1.81	0.215	0.524
Theoretically estimated fracture toughness K_{Cp} (MPa·m$^{1/2}$)	3.33	0.797	0.065	0.129

Fractography and binary-digitizing of size distribution of pores

Fracture surfaces were observed by a scanning electron microscope (SEM). Cross sections were also observed through an LSM to characterize spatial and size distributions of pores. Figure 3 shows examples of overall fracture surface observed by SEM. As seen in Figure 3(a), a typical morphology in fracture originated from a flaw is found in the dense material of Al-01. On the other hand, as seen in Figures 3(b), 3(c) and 3(d), which were observed respectively in porous materials of AL-35, AL-48 and AL-58, their fracture surfaces seem rough and featureless. Consequently, it is difficult to distinguish the fracture origin in porous materials. In these porous materials, clusters of pores were frequently observed. It has been reported that a similar morphology appears in porous ceramic materials (Hoshide, 1988).

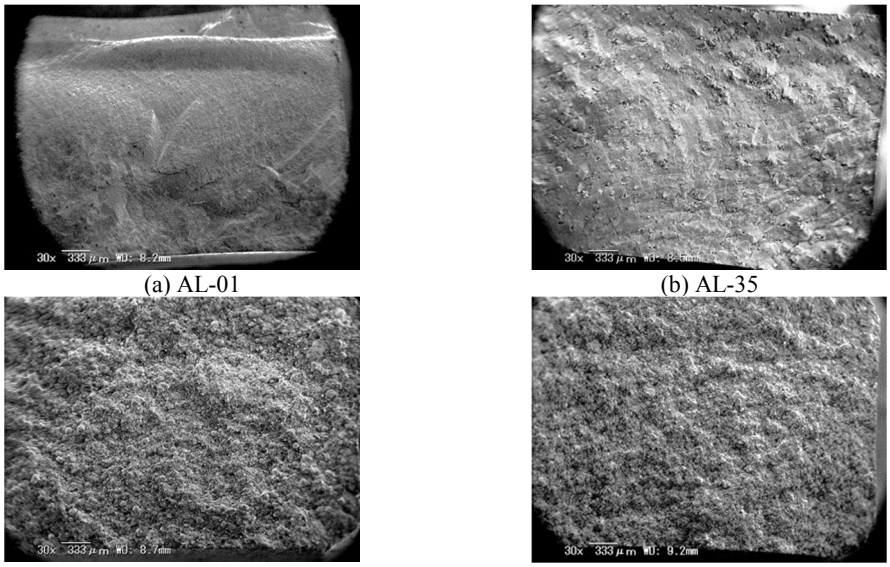

(a) AL-01 (b) AL-35

(c) AL-48 (d) AL-58

Fig. 3 - SEM photographs of fracture surfaces in respective materials

Figure 4 presents photographs observed by LSM. Pores are identified as white or light gray parts in Figure 4. Figure 5 shows images converted by binary-digitizing pictures in Figure 4. Pores are indicated by gray regions in Figure 5. It is seen that pore and its number in AL-58 are respectively smaller and more compared with those in AL-35 and AL-48.

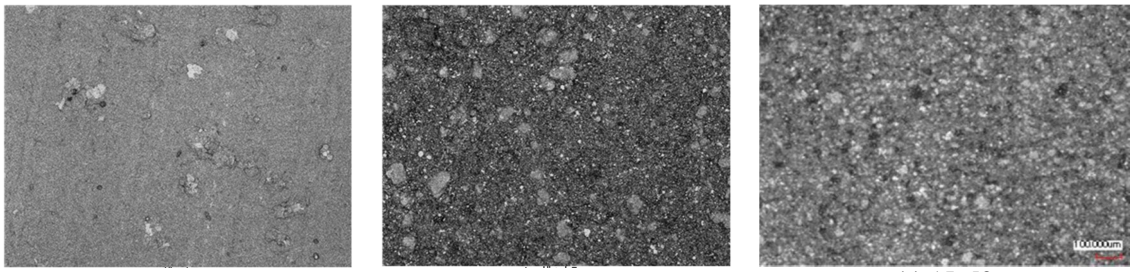

(a) AL-35 (b) AL-48 (c) AL-58

Fig. 4 - LSM photographs of surfaces on porous alumina ceramics

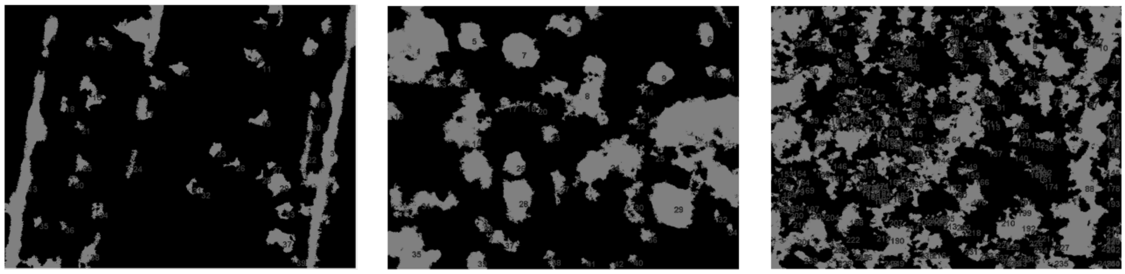

(a) AL-35 (b) AL-48 (c) AL-58

Fig. 5 - Binary-digitized pictures of surfaces on porous alumina ceramics

In this work, the shape of pore is presumed to be sphere, which implies a cross section of pore is expressed as a circle of radius a. Size and number of gray regions were measured by using a commercial software for particle analysis, and they are respectively converted to pore size a and density d_C of pores in cross section. The size distributions for pore are expressed by using three-parameter Weibull distribution function $F(a)$ as follows:

$$F(a) = 1 - \exp\left[-\left(\frac{a - a_L}{a_S} \right)^{\gamma} \right] \tag{3}$$

Scale parameter a_S, location parameter a_L and shape parameter γ, as well as density d_C of pores/cracks-size in each porous material are summarized in Table 4. The table also includes the other parameters the maximum pore radius a_{max} and average pore radius a_{ave} to be used in the following simulations.

Table 4 - Characteristics of pores/cracks-sizes and their distributions

Material	AL-01	AL-35	AL-48	AL-58
Density d_C (1/mm^2)	1.25	83.6	112	741
Shape parameter γ	7.7	1.3	0.97	0.87
Location parameter a_L (μm)	1.0	7.14	5.73	2.20
Scale parameter a_S (μm)	25	21.6	16.1	4.39
Maximum pore radius a_{max} (μm)	25	150	180	220
Average pore radius a_{ave} (μm)	0	63.0	58.9	42.6

NUMERICAL SIMULATION OF STRENGTH AFFECTED BY PORES

Modeling of flaws/pores

Inherent flaws generated in dense alumina AL-01 are distributed in a specimen, and pores are also distributed in specimens of porous alumina AL-35, AL-48 and AL-58. In this work, a fracture mechanics procedure to evaluate strength properties of porous alumina ceramics is proposed by presuming pores to be cracks.

In the simulation, such flaws/pores are modeled as circular, semi-elliptic or quarter-elliptic cracks. Cracks in a specimen are randomly located only within the region, which is subjected to tensile stress in the specimen under bending. It is assumed that the failure occurs when the maximum value, K_{max}, among all stress intensity factors in the specimen is just equal to the fracture toughness K_C of a material under consideration. As the result, one strength data for the specimen is obtained. Such a calculation is repeated to reach a specified number of specimens.

In determining positions of individual cracks, a Cartesian *x*-*y*-*z* coordinate is introduced within the tensile region of a specimen. In this coordinate, *x*- and *y*-axes are respectively parallel and vertical to the longitudinal direction of the specimen and *z*-axis is the transverse direction (width direction) of a specimen, as schematically illustrated in Figure 6. By considering no stress gradient in the width direction (*z*-axis) of specimen under bending mode, positions of cracks existing in an arbitrary cross section are projected in *z* direction and onto *x*-*y* plane. Therefore, in the simulation, the position (*x, y*) of a crack is prescribed on the *x*-*y* plane. For example, the position of *i*-th crack in a specimen is described as (x_i, y_i) on the *x*-*y* plane as shown in Figure 6. By using a series of quasi-uniform random numbers generated by a computer, crack positions are randomly set and the size *a* of each crack is given independently of its location.

According to crack position, cracks are classified into three types, i.e., embedded, surface, and corner cracks, which are schematically illustrated in Figure 7. The depth *h* of the center of an original circular crack is the distance from the specimen surface. The length *a* and *c* are radius of an original circular crack and the depth of a modeled crack, respectively.

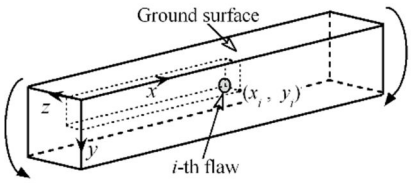

Fig. 6 - Cartesian coordinate in specimen subjected to bending

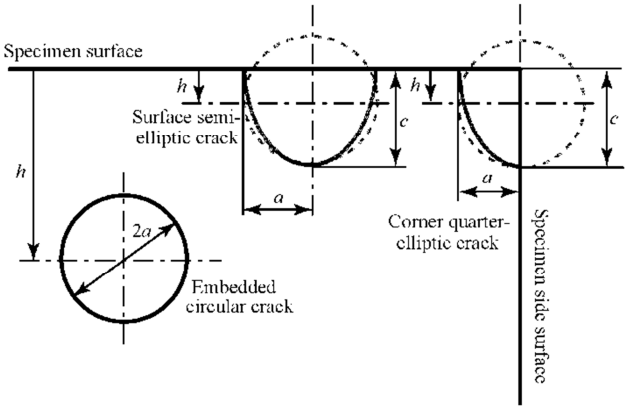

Fig. 7 - Schematic illustration of crack configurations; circular, semi-elliptic and quarter cracks

Fracture mechanics procedure

It has been reported (Hoshide, 1984, 1991, 1993, 1995) that a fracture-mechanics-based criterion for long cracks cannot be directly applied to the strength evaluation of ceramic components, which are fractured originating from small cracks. In this simulation, the following approximation (Hoshide, 1991) is adopted in the evaluation of a valid K value for a small crack with length a:

$$K = \sigma_{\mathrm{a}} \sqrt{\pi (a + l_0)} M_K \tag{4}$$

A length parameter l_0 is crack length to be added to the original crack length a. As for a pore, (4) implies the pore is surrounded by a virtual crack of length l_0. In (4), σ_{a} is the applied stress, and M_K is a magnification factor given by considering the shape and location of the crack as well as the stress distribution in a specimen. The value of M_K is determined using published numerical results (Murakami, 1987, 1992, 2001) according to the aforementioned situations of crack. The maximum $K_{\max}$ is obtained among all K values calculated for cracks located in a specimen, and the applied stress σ_{a} at the fracture of the specimen is designated as the strength σ_{f}. The fracture criterion, i.e., $K_{\max} = K_{\mathrm{C}}$, combined with (4) is written as follows:

$$\sigma_{\mathrm{a}} = \frac{K_{\mathrm{C}}}{\sqrt{\pi (a + l_0)} M_K} \tag{5}$$

Using (5), the strength value of one specimen is finally determined by the length a and the magnification factor M_{K} of crack dominating a fracture of the specimen.

Figure 8 shows the flow chart of the present simulation.

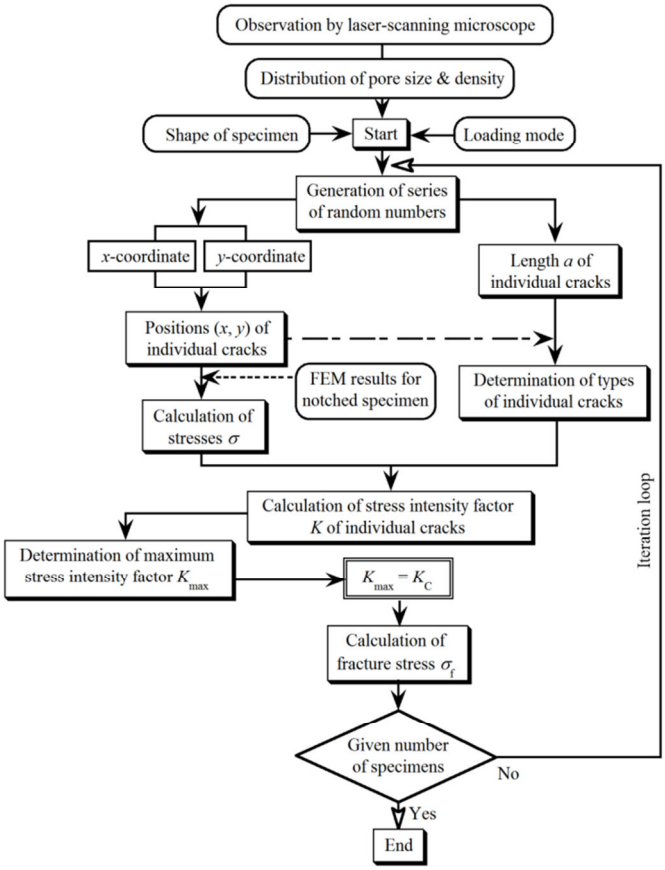

Fig. 8 - Flow chart of simulation

Parameters used in simulation

Size distributions and densities of cracks in AL-35, AL-48 and AL-58 listed in Table 4 are used in simulations, as aforementioned. As for AL-01 of high purity alumina, parameters used in a previous work (Hoshide, 2013) are applied for simulations. The number of surface cracks is given by the crack density and relative crack positions to the specimen surface, though corner cracks and surface cracks are not classified in the analysis. In this simulation, the ratio of corner cracks to total surface ones is set to be 0%.

Apparent fracture toughness has been determined experimentally by the procedure mentioned in a previous section. Since the toughness values are obtained by using straight-notched specimens in experiments, they are expected to be larger than actual ones. Therefore, in this work, the fracture toughness of a material with porosity p is estimated by using average pore radius $a_{p,\mathrm{ave}}$ and average bending strength $\sigma_{\mathrm{f,ave}}(p)$, based on fracture mechanics criterion. Fracture toughness K_{Cp} for material with porosity p is defined as follows.

$$K_{Cp} = \sigma_{\mathrm{f,ave}}(p)\,(\pi\, a_{p,\mathrm{ave}})^{1/2}\, M_K \tag{6}$$

In (6), M_K is a modification factor determined by crack geometry and loading mode. By setting $p = 0$ in (6), the fracture toughness K_{C0} of a non-porous material is given by using average pore radius $a_{0,\mathrm{ave}}$, and average bending strength $\sigma_{\mathrm{f,ave}}(0)$ in the material, as follows.

$$K_{C0} = \sigma_{f,ave}(0) \, (\pi \, a_{o,ave})^{1/2} \, M_K \tag{7}$$

Assuming M_K is a constant, the following relations are given from (6) and (7).

$$K_{Cp} = K_{C0} \, [\sigma_{f,ave}(p) \, / \, \sigma_{f,ave}(0)] \, (a_{p,ave} \, / \, a_{0,ave})^{1/2} \tag{8}$$

It should be remarked that purity of AL-58 is lower than those of the other materials. Therefore, in this simulation, the relation between porosity p and average strength $\sigma_{f,ave}(p)$ for the materials except for AL-58 is approximated as follows.

$$\sigma_{f,ave}(p) = \sigma_{f,ave}(0) \exp(-0.0894 \, p) \tag{9}$$

where

$$\sigma_{f,ave}(0) = 752 \tag{10}$$

By substitution of (9) for (8), fracture toughness in a material with porosity p is estimated as follows.

$$K_{Cp} = K_{C0} \exp(-0.0894 \, p) \, (a_{p,ave} \, / \, a_{0,ave})^{1/2} \tag{11}$$

Using the additional length l_0, crack length parameters $a_{0,ave}$ and $a_{p,ave}$ are defined as the following equations (12) and (13), respectively.

$$a_{0,ave} = l_0 \tag{12}$$

$$a_{p,ave} = a_{ave} + l_0 \tag{13}$$

In the above equations, a_{ave} is an average pore radius, which is observed experimentally. The maximum pore radius a_{max} as well as a_{ave} are shown in Table 4. Finally, a theoretically estimated fracture toughen K_{Cp} can be evaluated, and their values are listed in Table 3. Quantitative and qualitative orders of K_{Cp} are very similar to those of $K_{C,ap}$.

The modification using (4) is adopted in evaluating a K-value applicable to small flaw. The additional length l_0 in (4) is determined to be 10 μm based on theoretically estimated fracture toughness.

Procedure of simulation

A Monte Carlo simulation will be carried out for the same shape of specimen under the same loading mode as those arranged for the present experiment. In the present simulation, the loop calculation shown in Figure 8 is iterated 100 times for each type of the specimen. Actually, 100 trials are made by creating 100 different combinations of spatial and size distributions of cracks by using random numbers. Consequently, the simulation for each type of the specimen gives 100 strength data.

Simulated result and discussion

Figure 9 shows comparison of simulated and experimental strength. The dotted line presents a scatter band corresponding to a factor of $2^{1/2}$. Error bars in horizontal and vertical directions represent scatter ranges in simulated and experimental results, respectively. By comparing the simulated results with the experimental ones, a good coincidence is confirmed between them.

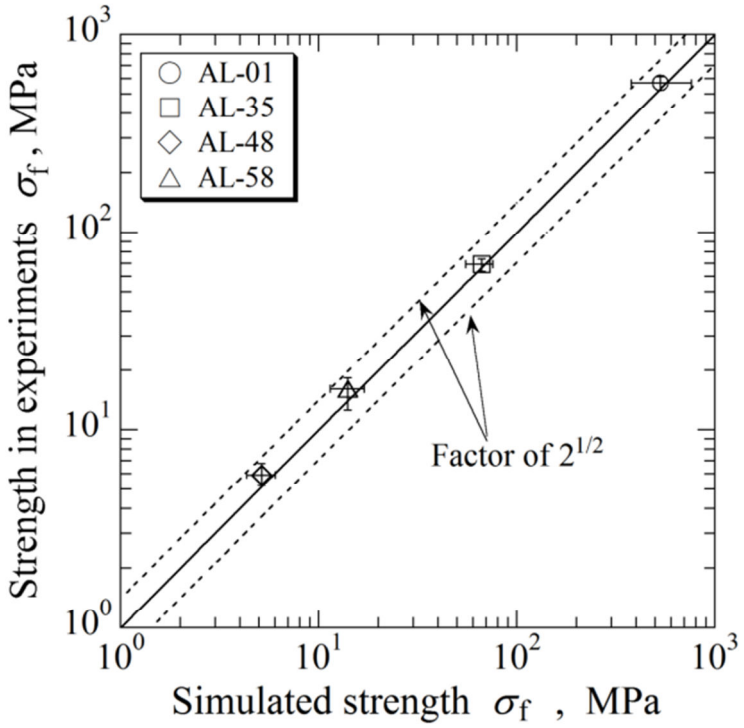

Fig. 9 - Comparison of simulated strength with experimental result

Although stress concentrations at tips of a pore and a crack are different, pores are treated as cracks in this simulation. Another assumption is that pores are presumed to be surrounded by virtual cracks. However, strength properties of porous alumina are adequately explained by the proposed procedure based on fracture mechanics. This suggests the proposed procedure is applicable to strength evaluation in porous ceramic materials.

CONCLUSIONS

In this work, the influences of porosity p, and of spatial and size distributions of pores on the porous ceramics strength were investigated based on experimental results observed by using dense alumina and three porous alumina with p = 34.9%, 48.4% and 57.8%. Strength characteristics in alumina with different porosity were obtained by three-point bending tests. As a general trend, it was clarified that strength was remarkably decreased with increase in porosity. However, strength in a material with p = 57.8% was found to be higher than strength in a material with p = 48.4%. As a result of observation of the specimens and fracture surfaces, pores smaller than those in the other materials were seen in the specimen with p = 57.8%. Consequently, it was suggested that strength characteristics were essentially affected by spatial and size distributions of pores rather than bulk porosity.

An analytical procedure based on fracture mechanics was proposed by using observed pore-distribution. The pore distributions were characterized by binary-digitizing images observed via a laser scanning microscope. In the analytical procedure, it was presumed that a pore was surrounded by a virtual crack and the characteristics of crack distribution were the same as those of pore distribution in respective material. A Monte Carlo simulation was conducted 100 times for a given material under 3-point bending. Simulated results revealed that the effects of porosity and of special and size distributions on the strength of porous alumina were well explained by using the analytical procedure proposed in this work.

ACKNOWLEDGMENTS

The authors thank Mr. Nakamura for his help in experiments.

REFERENCES

[1] Eugene R. Compression strength of porous sintered alumina and zirconia. J Amer Ceramic Soc, 1953, 36(2), pp. 65-68.

[2] Hoshide T, Fukui T, Yamada T. Effect of porosity on strength of zirconia refractory. J Soc Mater Sci, Japan, 1988, 37(421), pp. 1139-1145.

[3] Kawai C, Yamakawa A. Effect of porosity and microstructure on the strength of Si_3N_4: Designed microstructure for high strength, high thermal shock resistance, and facile machining. J Amer Ceramic Soc, 1997, 80(10), pp. 2705-2708.

[4] Testing method for flexural strength (modulus of rupture) of fine ceramics at room temperature, JIS R 1601. Japanese industrial standard, Japanese standards association, 2008.

[5] Weibull W. A statistical theory of the strength of materials. Ingeniors Vetenskaps Akademiens Handlingar Nr 151, 1939.

[6] Ashby MF, Jones DRH. Engineering Materials – An Introduction to their Properties and Applications, Oxford, Pergamon Press, 1980, p. 81.

[7] Hoshide T. Interrelation analyses of mechanical properties in commercial ceramics using cataloged data. Mater Sci Res Int, 1998, 4(3), pp. 179-185.

[8] Hoshide T, Furuya H, Nagase Y, Yamada T. Fracture mechanics approach to evaluation of strength in sintered silicon nitride. Int J Fract, 1984, 26, pp. 229-239.

[9] Hoshide T, Inoue T. Simulation of anomalous behavior of a small flaw in strength of engineering ceramics. Eng Fract Mech, 1991, 38, pp. 307-312.

[10] Hoshide T. Grain fracture model and its application to strength evaluation in engineering ceramics. Eng Fract Mech, 1993, 44, pp. 403-408.

[11] Hoshide T, Masuda M. Dependence of strength on size of flaw dominating fracture in ceramics. Mater Sci Res Int, 1995, 1, pp. 108-113.

[12] Murakami Y, Aoki A, Hasebe N, Itoh Y, Miyata H, Miyazaki N, et al. Stress intensity factors handbook Vol 1&2: Oxford, Pergamon Press, 1987.

[13] Murakami Y, Hanson MT, Hasebe N, Itoh Y, Kishimoto K, Miyata H, et al. Stress intensity factors handbook Vol 3: The Society of Materials Science, Japan, and Pergamon press, 1992.

[14] Murakami Y, Hasebe N, Itoh Y, Kishimoto K, Miyata H, Miyazaki N, et al. Stress intensity factors handbook Vols. 4 and 5: The Society of Materials Science, Japan, and Elsevier science, 2001.

[15] Hoshide T, Sugiyama H. Numerical analysis of sample-size effect on strength of alumina. J Mater Eng Perform, 2013, 22(1), pp. 1-8.